of HCV and Rep helicases reveal structural similarities between SF1 and SF2 super-families of helicases. *Protein Sci.* **7,** 605–610 (1998).
12. Vale, R. D. & Milligan, R. A. The way things move: looking under the hood of molecular motor proteins. *Science* **288,** 88–95 (2000).
13. Bartenschlager, R. The NS3/4A proteinase of the hepatitis C virus: unravelling structure and function of an unusual enzyme and a prime target for antiviral therapy. *J. Viral Hepat.* **6,** 165–181 (1999).
14. Gallinari, P. *et al.* Multiple enzymatic activities associated with recombinant NS3 protein of hepatitis C virus. *J. Virol.* **72,** 6758–6769 (1998).
15. Pang, P. S., Jankowsky, E., Planet, P. J. & Pyle, A. M. The hepatitis C viral NS3 protein is a processive DNA helicase with cofactor enhanced RNA unwinding. *EMBO J.* **21,** 1168–1176 (2002).
16. Paolini, C., De Francesco, R. & Gallinari, P. Enzymatic properties of hepatitis C virus NS3-associated helicase. *J. Gen. Virol.* **81,** 1335–1345 (2000).
17. Lucius, A. L., Maluf, N. K., Fischer, C. J. & Lohman, T. M. General methods for analysis of sequential "n-step" kinetic mechanisms: application to single turnover kinetics of helicase-catalyzed DNA unwinding. *Biophys. J.* **85,** 2224–2239 (2003).
18. Ali, J. A. & Lohman, T. M. Kinetic measurement of the step size of DNA unwinding by *Escherichia coli* UvrD helicase. *Science* **275,** 377–380 (1997).
19. Bianco, P. R. & Kowalczykowski, S. C. Translocation step size and mechanism of the RecBC DNA helicase. *Nature* **405,** 368–372 (2000).
20. Jankowsky, E., Gross, C. H., Shuman, S. & Pyle, A. M. The DExH protein NPH-II is a processive and directional motor for unwinding RNA. *Nature* **403,** 447–451 (2000).
21. Bianco, P. R. *et al.* Processive translocation and DNA unwinding by individual RecBCD enzyme molecules. *Nature* **409,** 374–378 (2001).
22. Ha, T. *et al.* Initiation and re-initiation of DNA unwinding by the *Escherichia coli* Rep helicase. *Nature* **419,** 638–641 (2002).
23. Spies, M. *et al.* A molecular throttle: the recombination hotspot chi controls DNA translocation by the RecBCD helicase. *Cell* **114,** 647–654 (2003).
24. Dessinges, M. N., Lionnet, T., Xi, X. G., Bensimon, D. & Croquette, V. Single-molecule assay reveals strand switching and enhanced processivity of UvrD. *Proc. Natl Acad. Sci. USA* **101,** 6439–6444 (2004).
25. Lucius, A. L. *et al.* DNA unwinding step-size of *E. coli* RecBCD helicase determined from single turnover chemical quenched-flow kinetic studies. *J. Mol. Biol.* **324,** 409–428 (2002).
26. Levin, M. K. & Patel, S. S. The helicase from hepatitis C virus is active as an oligomer. *J. Biol. Chem.* **274,** 31839–31846 (1999).
27. Locatelli, G. A., Spadari, S. & Maga, G. Hepatitis C virus NS3 ATPase/helicase: an ATP switch regulates the cooperativity among the different substrate binding sites. *Biochemistry* **41,** 10332–10342 (2002).
28. Levin, M. K., Wang, Y. H. & Patel, S. S. The functional interaction of the hepatitis C virus helicase molecules is responsible for unwinding processivity. *J. Biol. Chem.* **279,** 26005–26012 (2004).
29. Kawaoka, J., Jankowsky, E. & Pyle, A. M. Backbone tracking by the SF2 helicase NPH-II. *Nature Struct. Mol. Biol.* **11,** 526–530 (2004).
30. Kuzmic, P. Program DYNAFIT for the analysis of enzyme kinetic data: application to HIV proteinase. *Anal. Biochem.* **237,** 260–273 (1996).

Supplementary Information accompanies the paper on **www.nature.com/nature**.

Acknowledgements The authors would like to thank E. Jankowsky, J. Kawaoka and M. Brenowitz for discussions. We thank R. Beran for sharing his results on NS3 unwinding of multi-piece RNA substrates, and H. Le for discussions and early gifts of NS3 protein. This work was supported by grants from the NIH and the Howard Hughes Medical Institute. A.M.P. is an HHMI investigator.

Competing interests statement The authors declare that they have no competing financial interests.

Correspondence and requests for materials should be addressed to A.M.P. (anna.pyle@yale.edu).

Detection of an intermediate of photosynthetic water oxidation

Juergen Clausen & Wolfgang Junge

Division of Biophysics, Department of Biology/Chemistry, Universität Osnabrück, D-49069 Osnabrück, Germany

The oxygen that we breathe is produced by photosystem II of cyanobacteria and plants. The catalytic centre, a Mn_4Ca cluster, accumulates four oxidizing equivalents before oxygen is formed, seemingly in a single reaction step[1–8] $2H_2O \rightleftharpoons O_2 + 4H^+ + 4e^-$. The energy and cycling of this reaction derives solely from light. No intermediate oxidation product of water has been detected so far. Here, we shifted the equilibrium of the terminal reaction backward by increasing the oxygen pressure and monitoring (by absorption transients in the near-ultraviolet spectrum) the electron transfer from bound water into the catalytic centre. A tenfold increase of ambient oxygen pressure (2.3 bar) half-suppressed the full progression to oxygen. The remaining electron transfer at saturating pressure (30 bar) was compatible with the formation of a stabilized intermediate. The abstraction of four electrons from water was probably split into at least two electron transfers: mildly endergonic from the centre's highest oxidation state to an intermediate, and exergonic from the intermediate to oxygen. There is little leeway for photosynthetic organisms to push the atmospheric oxygen concentration much above the present level.

The catalytic centre of photosynthetic water oxidation is embedded in a protein, photosystem II (PSII), and is composed of a Mn_4Ca cluster and a redox-active tyrosine (Y_Z)[1–3]. Its structure is beginning to be clarified[4–6]. Absorption of a quantum of light drives a charge separation to yield an oxidized chlorophyll *a* entity ($P680^+$). It oxidizes Y_Z in nanoseconds and, from there on, the Mn_4Ca cluster in microseconds[2,7]. Three absorbed quanta clock the Mn_4Ca cluster through increasingly higher oxidation states, from the lowest, S_0, to S_1, S_2 and S_3. Dioxygen is liberated only after input of a forth quantum of light to yield $S_3Y_Z^{ox} = S_4$[8]. Up to the penultimate state (S_3) the substrate, bound water, is exchangeable with isotope-labelled bulk water[9,10]. The production of potentially dangerous oxidation intermediates of water seems to be avoided by concentrating the fourfold oxidation of two bound water molecules into a single terminal reaction, $S_4(H_2O)_2 \rightarrow S_0Y_Z + O_2 + \text{protons}$. Despite intensive search, oxidized intermediates of water (for example, the postulated peroxide[11]) have escaped detection[12]. There are three factors indicative of the terminal reaction sequence, from start to end, which evolve with the same velocity: (1) the reduction of Y_Z^{ox} as detected by electron paramagnetic resonance[13]; (2) the reduction of Mn_4CaY_Z (by bound water), as detected by ultraviolet flash spectrophotometry[14–17]; and (3) the liberation of oxygen, as detected by rapid polarography[12,17,18]. The terminal reaction sequence is probably rate-limited by the transfer of the first electron into $S_3Y_Z^{ox}$. Intermediates might have escaped detection because of their short lifetime.

We attempted to stabilize intermediates by increasing the partial pressure of oxygen over the reaction mixture. This approach is illustrated by a sequential reaction with only one

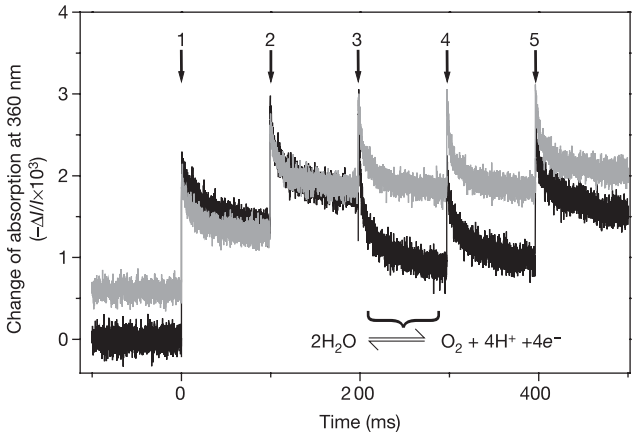

Figure 1 Ultraviolet absorption transients at a wavelength of 360 nm of dark-adapted PSII core particles under excitation with five short laser flashes (arrows). Black trace, air; grey trace, 20 bar oxygen. The undershoot after the third flash (black trace) reflects the relaxation of the fourfold oxidized catalytic centre culminating in the release of oxygen (see text).

intermediate, B:

$$A \underset{b}{\overset{a}{\rightleftharpoons}} B \underset{d}{\overset{c}{\rightleftharpoons}} C + O_2 + \text{protons} \quad (1)$$

which may be tentatively read as:

$$S_3Y_z^{ox}(H_2O)_2 \underset{b}{\overset{a}{\rightleftharpoons}} S_2Y_zH_2O_2 \underset{d}{\overset{c}{\rightleftharpoons}} S_0Y_z + O_2 + \text{protons} \quad (2)$$

$a - d$ denote the forward and backward rate constants, and H_2O_2 stands for the hypothetical peroxide intermediate. The choice of only a single intermediate and its assignment to S_2-peroxide is arbitrary but plausible. All reactions are pseudo-first order, except for the last back reaction (second-order rate constant d). With S_i representing solid state components, and water being both reagent and solvent, oxygen and protons are the only dilute reaction partners. The involvement of protons was neglected in the following for simplicity. We varied the oxygen concentration to change the equilibrium between the intermediate (B) and the fully relaxed state (C).

Figure 1 shows absorption transients at a wavelength of 360 nm under excitation of dark-adapted PSII core particles with a train of five laser flashes. These transients reflect redox reactions of manganese and of intrinsic and extrinsic electron acceptors of PSII, as documented in the literature[17,19] (see also Supplementary Fig. 2). Both traces were recorded at pH 6.7, the first at ambient oxygen pressure (black) and the second at 20 bar oxygen (grey). The most interesting feature of the control trace (black) is the decrease in the absorption transient upon the third flash of light, which hereafter we call the undershoot. It is caused by an exponential decay component with a half-life of typically 1.3 ms (20 °C). It compensates the upward-directed jumps at flashes 1 and 2 (see Supplementary Information) and is directly related to oxygen evolution[12,14–17,20]. In PSII particles from *Synechocystis*, as used in this work, the equilibrium of the oxidation states in the dark is $0.3/0.7/0/0 = S_0/S_1/S_2/S_3$ (refs 12, 21). Thus, oxygen evolution and the concomitant undershoot of absorption appear only at and after the third flash of light, and are absent at the former two flashes[17,21]. Comparison of the two traces in Fig. 1 reveals that the undershoot is suppressed at high oxygen pressure (grey transient).

There are more differences between the two traces in Fig. 1: (1) the magnitude of the upshot at the first flash differed because of a different proportion of incompetent centres in oxygen evolution (see Supplementary Information), and (2) the non-oscillating signals at flashes 4 and 5, and further on, at high oxygen pressure. We tentatively interpreted the latter as a cycling of <100 ms between states S_3Y^{ox} and S_3Y at the donor side of PSII, similar to that which occurs in Mn-depleted PSII core particles.

Figure 2 shows the original transients of flashes 2 and 3 under three conditions: with ambient oxygen pressure (0.21 bar); with elevated oxygen pressure (20 bar); and with elevated nitrogen pressure and no oxygen present (19 bar N_2, only a few smoothed points displayed). It is evident that the undershoot was diminished by elevated oxygen pressure, but not by pressure *per se*. In contrast to the decay after the third flash, the decay after the second flash was not affected by the elevated oxygen pressure, implying that the dark equilibrium between oxidation states was not perturbed. The effects caused by exposure to 30 bar oxygen were reversible. After 30 min exposure to 20 bar O_2 and slow re-establishment of the ambient pressure (over 5 h at 0 °C), samples still revealed typically 70–80% of their original oxygen-evolving activity under continuous illumination. Similarly, the normal oscillatory behaviour under excitation of dark-adapted material with a group of light flashes was restored by decompression to the ambient oxygen level. This is documented in the Supplementary Information.

The effects of increased oxygen pressure were immediately apparent on visual inspection of the raw data. The ultraviolet transients at the third laser flash were normalized to yield the same extent of the rapid rise, and corrected (see Methods and Fig. 3). The normalized and corrected transients at 360 nm at the third laser flash reflect the electron transfer into the catalytic centre after reaching state S_4. Three corrected traces (at 0.21, 1 and 20 bar O_2) are documented in Fig. 3. We titrated their extent as a function of the oxygen pressure (see Fig. 4, points). The extrapolated saturation level of the suppression by high oxygen pressure was 83% (dashed line) and the midpoint was at 2.3 bar.

The solid line in Fig. 4 was calculated on the basis of the tentatively chosen reaction scheme (equation (1)) involving only a single intermediate. Initially (that is, right after the third laser flash) the concentrations of A, B and C were $A_0 = 1$ and $B_0 = C_0 = 0$, and the new equilibrium was:

$$A_\infty = \left(1 + \frac{a}{b}\left(1 + \frac{c}{pd}\right)\right)^{-1}, \quad \frac{B_\infty}{A_\infty} = \frac{a}{b}, \quad \frac{C_\infty}{B_\infty} = \frac{c}{pd} \quad (3)$$

where p denotes the oxygen pressure and a, b, c and d the rate constant of the reaction scheme (equation (1)). The three species A,

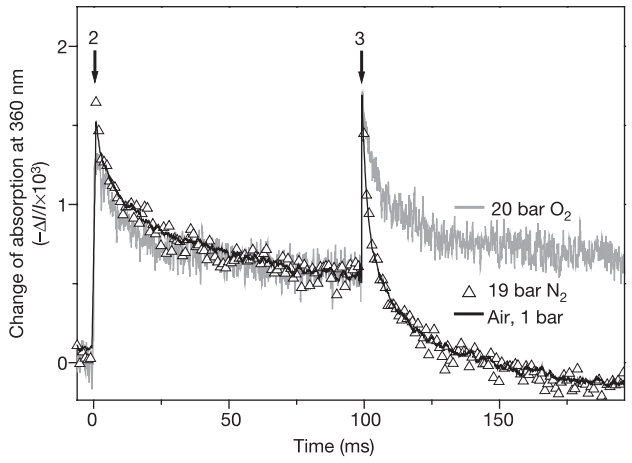

Figure 2 Ultraviolet absorption transients as induced by the second and third flash under variation of the gas composition and pressure. The undershoot indicating the formation of oxygen is clearly depressed by 20 bar O_2 but is unaffected by enhanced hydrostatic pressure alone (19 bar N_2). The control trace (air) is smoothed over 30 points, whereas the other traces are smoothed over five points.

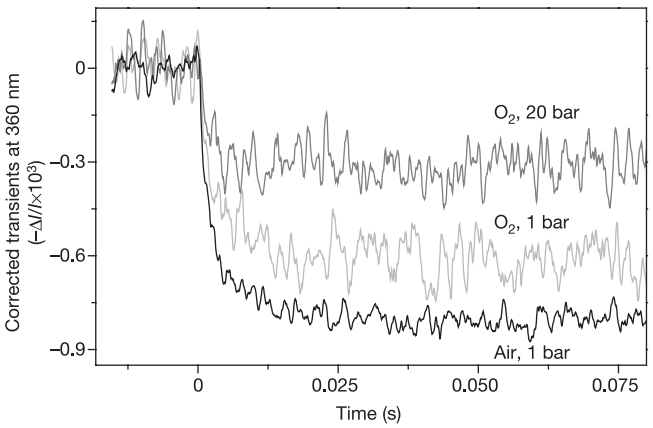

Figure 3 Electron transfer into the catalytic Mn_4Ca centre at three different oxygen pressures, and corrected ultraviolet absorption transients at the third flash. Each data point represents the difference between the respective points at the third and the second flash (as shown in Fig. 2), serving to eliminate the contribution at the chosen wavelength (360 nm) of the consecutive reactions of the added electron acceptor (2,5-dichloro-*p*-benzochinon). A further correction was introduced for the underlying step-shaped signal attributable to the transition $S_2 \rightarrow S_3$ on the second flash. Original data were smoothed over 20 points.

B and C could not be monitored separately, and together they contributed to the corrected ultraviolet transient at the third flash of light. We discuss the expected behaviour in terms of equation (2), wherein the intermediate is assumed to be $S_2Y_ZH_2O_2$. This is only one of several choices, as mentioned. The decay of absorption reverses two positive jumps of equal magnitude during the foregoing univalent oxidation steps, $S_1 \rightarrow S_2$ and $S_2 \rightarrow S_3$ (refs 22–24) (see Supplementary Information). In contrast to the former, the transitions $Y_Z \rightarrow Y_Z^{ox}$ and $S_0 \rightarrow S_1$ marginally contribute at this wavelength (360 nm)[22]. Accordingly, the disappearance of $A = S_3Y_Z^{ox}(H_2O)_2$, the highest oxidation state of the centre, is expected to cause absorption twice as large as the same amount of an intermediate in the second oxidation state, $B = S_2Y_ZH_2O_2$.

We interpreted the corrected ultraviolet transient, therefore, as reflecting the behaviour of the composite observable, X, as a function of the oxygen pressure (p):

$$X = A + \frac{1}{2}B = f(p) \tag{4}$$

Insertion of equation (3) into equation (4) yielded the documented fit (solid line) to the titration data in Fig. 4. The fit parameter values were $a/b = 0.5$, $c/d = 6.8$ bar and $p_{1/2} = 2.3$ bar.

The expected time course at very high oxygen pressure ($p \rightarrow \infty$) is given by:

$$X(t) = \frac{1}{2}\left(1 + \frac{1}{a+b}(b + ae^{-(a+b)t})\right) \tag{5}$$

It is a mono-exponential decay with a rate constant, k:

$$k = a + b \tag{6}$$

At 20 bar O_2 the observed half-decay time of the signal was 0.8 ms (data fit by single exponential), implying a rate constant of $k = 866\,s^{-1}$, so that $a = 144\,s^{-1}$ and $b = 722\,s^{-1}$. The absolute values of the rate constants of the second partial reaction, c and dp, could not be determined, but both were much larger than a and b.

With these parameters, which were based on data obtained at pH 6.7 and at 20 °C, the standard free energy profile of the reaction sequence (equation (1)) could be calculated (see equation (3)) according to the relation $\Delta G^0 = -RT \ln K$, where RT is as usual and K denotes the equilibrium constant.

$$\Delta G^{0'}_{AB} \cong +1.7\,kJ\,mol^{-1}, \quad \Delta G^{0'}_{BC} \cong -4.7\,kJ\,mol^{-1} \tag{7}$$

Both values relate to the production of 1 mol dioxygen under pseudo-standard conditions (≈pH 6.7, 1 bar O_2, 20 °C). This free energy profile is illustrated in the insert to Fig. 4. At ambient pressure (0.21 bar oxygen) ΔG_{BC} would be $-8.6\,kJ\,mol^{-1}$. The role of proton release in the final reaction sequence will be detailed elsewhere. Here, we only mention that the second partial reaction ($B \rightarrow C$) involves the liberation into the bulk of one proton per O_2. This will be detailed elsewhere (see refs 17, 25–28 for surveys of the proteolytic reactions).

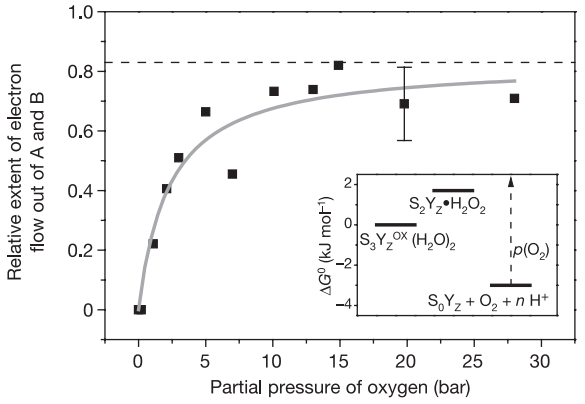

Figure 4 Titration of the corrected absorption transients by elevated oxygen pressure (see text and equation (4)). The insert illustrates the calculated standard free energy profile starting from the highest oxidation state, continuing through the peroxide intermediate, to the fully relaxed state with released oxygen. The error bar denotes the standard deviation of data from 20 experiments with material from six preparations.

Our experiments demonstrate the back pressure of oxygen on the Mn_4Ca centre. It would be interesting to re-investigate the previously reported oxygen consumption by PSII[29] (under ambient pressure) under conditions of varied oxygen pressure.

Production of oxygen through photosynthetic water oxidation is a process of paramount biological importance and technical relevance. It operates at extremely positive redox potential (>+1.2 V; refs 25, 30). We present experimental evidence for an intermediate of the enigmatic reaction pathway from water to oxygen. The free energy drop at the very end of this reaction is rather small. It emphasizes that PSII operates at the outermost redox span that can be driven by quanta of red light. The unexpectedly low pressure that half-suppresses oxygen evolution (2.3 bar at pH 6.7) has an interesting consequence. The present atmospheric pressure of oxygen is close to the expected obtainable maximum. It approaches it rather closely when taking into consideration the additional effect of pH: the luminal side of the thylakoid membrane is more acidic than the pH 6.7 used in our experiments. □

Methods

PSII core particles and media

Oxygen-evolving PSII core particles were prepared as described[21] from modified WT* cells of *Synechocystis sp.* PCC6803 (ref. 21). For flash-spectrometric measurements PSII core particles were suspended in standard medium (1 M sucrose, 25 mM $CaCl_2$, 10 mM NaCl, 1 M glycine betaine, 0.06% (w/v) *N*-Dodecyl-β-D-maltoside, 50 mM 2-(*N*-Morpholino)ethanesulphonic acid, pH 6.7). The temperature was 20 ± 0.5 °C.

Samples under high pressure

An optical cell with fused quartz windows was constructed to sustain pressures up to 30 bar. Standard reaction medium was pre-equilibrated with purified oxygen or nitrogen gas under the desired partial pressure for at least 40 min. It was then filled into the optical cell and re-equilibrated with the pressurized gas phase for another 10 min. A small aliquot (typically 50 µl) of dark-adapted PSII particles from the concentrated stock was injected into the cell (roughly 3 ml liquid, 20 ml gas). The mixture was kept in darkness and equilibrated at the chosen pressure for another 20 min under gentle stirring. After addition, under pressure, of the electron acceptor the sample was excited with a group of laser flashes and ultraviolet absorption transients were recorded.

Laser excitation and spectrophotometry

Samples contained in the pressure-controlled optical cell were excited with a series of flashes from a Q-switched Nd-YAG laser (wavelength 532 nm, duration 6 ns full width at half maximum (FWHM), saturating energy, 100 ms between flashes). Absorption transients were monitored at a wavelength of 360 nm. This wavelength was chosen to reveal charge transfer bands of the Mn_4Ca cluster with minimal contributions from tyrosine, Y_Z (see spectra in Supplementary Information). Data were recorded at an analogue bandwidth of 10 kHz, digitized at 50 µs per bin, and digitally smoothed when indicated in the figure legends.

Received 26 February; accepted 18 May 2004; doi:10.1038/nature02676.

1. Barber, J. Photosystem II: the engine of life. *Q. Rev. Biophys.* **36,** 71–89 (2003).
2. Renger, G. Photosynthetic water oxidation to molecular oxygen: apparatus and mechanism. *Biochim. Biophys. Acta* **1503,** 210–228 (2001).
3. Robblee, J. H., Cinco, R. M. & Yachandra, V. K. X-ray spectroscopy-based structure of the Mn cluster and mechanism of photosynthetic oxygen evolution. *Biochim. Biophys. Acta* **1503,** 7–23 (2001).
4. Zouni, A. *et al.* Crystal structure of photosystem II from *Synechococcus elongatus* at 3.8 Å resolution. *Nature* **409,** 739–743 (2001).
5. Kamiya, N. & Shen, J. R. Crystal structure of oxygen-evolving photosystem II from *Thermosynechococcus vulcanus* at 3.7-angstrom resolution. *Proc. Natl Acad. Sci USA* **100,** 98–103 (2003).
6. Ferreira, K. N., Iverson, T. M., Maghlaoui, K., Barber, J. & Iwata, S. Architecture of the photosynthetic oxygen-evolving center. *Science* **303,** 1831–1838 (2004).
7. Rutherford, A. W. Photosystem II, the water-splitting enzyme. *Trends Biochem. Sci.* **14,** 227–232 (1989).
8. Kok, B., Forbush, B. & McGloin, M. Cooperation of charges in photosynthetic O_2 evolution - I. A linear four-step mechanism. *Photochem. Photobiol.* **11,** 457–475 (1970).
9. Hendry, G. & Wydrzynski, T. O-18 isotope exchange measurements reveal that calcium is involved in the binding of one substrate-water molecule to the oxygen-evolving complex in photosystem II. *Biochemistry* **42,** 6209–6217 (2003).
10. Hillier, W., Messinger, J. & Wydrzynski, T. Kinetic determination of the fast exchanging substrate water molecule in the S_3 state of photosystem II. *Biochemistry* **37,** 16908–16914 (1998).

11. Renger, G. in *Photosynthetic Oxygen Evolution* (ed. Metzner, H.) 229–248 (Academic, London, 1978).
12. Clausen, J., Debus, R. J. & Junge, W. Time-resolved oxygen production by PSII: Chasing chemical intermediates. *Biochim. Biophys. Acta* **1655,** 184–194 (2004).
13. Babcock, G. T., Blankenship, R. E. & Sauer, K. Reaction kinetics for positive charge accumulation on the water side of chloroplast photosystem II. *FEBS Lett.* **61,** 286–289 (1976).
14. Dekker, J. P., Plijter, J. J., Ouwehand, L. & van Gorkom, H. J. Kinetics of manganese redox transitions in the oxygen evolving apparatus of photosynthesis. *Biochim. Biophys. Acta* **767,** 176–179 (1984).
15. Renger, G. & Weiss, W. Studies on the nature of the water oxidizing enzyme. III. Spectral characterization of the intermediary redox states in the water-oxidizing enzyme system Y. *Biochim. Biophys. Acta* **850,** 184–196 (1986).
16. Saygin, Ö. & Witt, H. T. Optical characterization of intermediates in the water-splitting enzyme system of photosynthesis—possible states and configurations of manganese and water. *Biochim. Biophys. Acta* **893,** 452–469 (1987).
17. Haumann, M., Bögershausen, O., Cherepanov, D. A., Ahlbrink, R. & Junge, W. Photosynthetic oxygen evolution: H/D isotope effects and the coupling between electron and proton transfer during the redox reactions at the oxidizing side of photosystem II. *Photosynth. Res.* **51,** 193–208 (1997).
18. Hundelt, M., Hays, A. M., Debus, R. J. & Junge, W. Oxygenic photosystem II: the mutation D1-D61N in *Synechocystis* sp. PCC 6803 retards S-state transitions without affecting electron transfer from Y_Z to P_{680}^+. *Biochemistry* **37,** 14450–14456 (1998).
19. Karge, M., Irrgang, K. D. & Renger, G. Analysis of the reaction coordinate of photosynthetic water oxidation by kinetic measurements of 355 nm absorption changes at different temperatures in photosystem II preparations suspended in either H_2O or D_2O. *Biochemistry* **36,** 8904–8913 (1997).
20. Rappaport, F., Blanchard-Desce, M. & Lavergne, J. Kinetics of electron transfer and electrochromic change during the redox transition of the photosynthetic oxygen-evolving complex. *Biochim. Biophys. Acta* **1184,** 178–192 (1994).
21. Clausen, J. *et al.* Photosynthetic water oxidation: Mutations of D1-Glu189K, R and Q of *Synechocystis* sp. PCC6803 are without any influence on electron transfer rates at the donor side of photosystem II. *Biochim. Biophys. Acta* **1506,** 224–235 (2001).
22. Lavergne, J. Improved UV-visible spectra of the S-transitions in the photosynthetic oxygen-evolving system. *Biochim. Biophys. Acta* **1060,** 175–188 (1991).
23. Dekker, J. P. in *Manganese Redox Enzymes* (ed. Pecoraro, V. L.) 85–104 (VCH Publishers, New York, 1992).
24. Haumann, M., Drevenstedt, W., Hundelt, M. & Junge, W. Photosystem II of green plants: Oxidation and deprotonation of the same component (histidine?) on $S_1^* \rightarrow S_2^*$ in chloride depleted centers as on $S_2 \rightarrow S_3$ in controls. *Biochim. Biophys. Acta* **1273,** 237–250 (1996).
25. Rappaport, F. & Lavergne, J. Coupling of electron and proton transfer in the photosynthetic water oxidase. *Biochim. Biophys. Acta* **1503,** 246–259 (2001).
26. Jahns, P., Lavergne, J., Rappaport, F. & Junge, W. Stoichiometry of proton release during photosynthetic water oxidation: a reinterpretation of the response of Neutral red leads to a non-integer pattern. *Biochim. Biophys. Acta* **1057,** 313–319 (1991).
27. Lavergne, J. & Junge, W. Proton release during the redox cycle of the water oxidase. *Photosynth. Res.* **38,** 279–296 (1993).
28. Junge, W., Haumann, M., Ahlbrink, R., Mulkidjanian, A. & Clausen, J. Electrostatics and proton transfer in photosynthetic water oxidation. *Phil. Trans. R. Soc. Lond. B* **357,** 1407–1417 (2002).
29. Beck, W. F., de Paula, J. C. & Brudvig, G. W. Active and resting state of the O2-evolving complex of Photosystem II. *Biochemistry* **24,** 3035–3043 (1985).
30. Klimov, V. V., Allakhverdiev, S. I., Demeter, S. & Krasnovsky, A. A. Photoreduction of pheophytin in the photosystem II of chloroplasts with respect to the redox potential of the medium. *Dokl. Akad. Nauk SSSR* **249,** 227–230 (1979).

Supplementary Information accompanies this paper on **www.nature.com/nature**.

Acknowledgements We thank H. Kenneweg for technical assistance, H. Heine for advice on the construction of the pressure cell, R. Debus for cooperation on *Synechocystis*, and R. Ahlbrink and A. Mulkidjanian for discussions and help. This work was financially supported by the Deutsche Forschungsgemeinschaft, the Fonds der Chemischen Industrie and the Land Niedersachsen.

Competing interests statement The authors declare that they have no competing financial interests.

Correspondence and requests for materials should be addressed to W.J. (junge@uos.de).

addendum

Measuring fast neutrons in Hiroshima at distances relevant to atomic-bomb survivors

T. Straume, G. Rugel, A. A. Marchetti, W. Rühm, G. Korschinek, J. E. McAninch, K. Carroll, S. Egbert, T. Faestermann, K. Knie, R. Martinelli, A. Wallner, C. Wallner, S. Fujita[1], K. Shizuma[2], M. Hoshi[3] & H. Hasai[4]

[1]*Department of Statistics, Radiation Effects Research Foundation, 5-2 Hijiyama Park, Minami-ku, Hiroshima 732-0815, Japan*
[2]*Quantum Energy Applications, Graduate School of Engineering, Hiroshima University, Higashi-Hiroshima 739-8527, Japan*
[3]*International Radiation Information Center, Research Institute for Radiation, Biology and Medicine, Hiroshima University, 1-2-3 Kasumi, Minami-ku Hiroshima 734-8553, Japan*
[4]*Hiroshima Kokusai Gakuin University, 6-20-1 Nakano, Aki-ku, Hiroshima 739-0321, Japan*

We wish to clarify misunderstandings created by our Letter on the measurement of Hiroshima fast neutrons[1]. Our measurements were partly made within the framework of (and contributed to) a comprehensive reassessment of A-bomb dosimetry conducted by the Joint US–Japan Working Group that produced the new RERF DS02 Dosimetry System, soon to be published[2,3]. Also, our speculation[1] concerning a "slightly underestimated height-of-burst (HOB) for the Hiroshima bomb" does not imply that the HOB should be changed based solely on the ^{63}Ni measurements. Although our work provides direct information on dose-relevant fast-neutron fluence, it should not be construed to be the sole basis for resolution of the Hiroshima neutron discrepancy that had been reported for thermal neutrons. The original authors were not fully aware of the scientific input of the copper sampling in Hiroshima and wish to remedy this here by extending the author list and by acknowledging additional support from Japanese funding agencies (Grants-in-Aid for Scientific Research B and C of the Japan Ministry of Education, Culture, Sports, Science and Technology for support and the Radiation Effects Research Foundation (RERF) in Hiroshima for the copper sampling effort). □

1. Straume, T. *et al.* Measuring fast neutrons in Hiroshima at distances relevant to atomic-bomb survivors. *Nature* **424,** 539–542 (2003).
2. Cullings, H. M. & Fujita, S. The way to DS02: resolving the neutron discrepancy. *RERF Update* **14,** 17–23 (2003).
3. *DS02: A New Dosimetry System for A-Bomb Survivor Studies* Joint Senior Review Group Report on DS02 ⟨http://tis.eh.doe.gov/health/ihp/japan/DS02.pdf⟩ (March 2003).